Micromanipulation of Langmuir-Monolayers with Optical Tweezers

S. Wurlitzer,[†] C. Lautz,[‡] M. Liley,[§] C. Duschl,[||] and Th. M. Fischer*,[⊥]

Fakultät für Physik, Universität Leipzig, Linnéstr. 5, 04103 Leipzig, Germany, Newport GmbH, Holzhofallee 19, 64295 Darmstadt, Germany, CSEM SA, Jaquet-Droz 1, CH-2007 Neuchâtel, Switzerland, Laboratoire de Chimie Physique des Polymères et Membranes, Département de Chimie, Ecole Polytechnique Fédérale de Lausanne - (EPFL) CH-1015 Lausanne, Switzerland, and Max Planck Institute of Colloids and Interfaces, Am Mühlenberg 1, 14476 Golm, Germany

Received: July 6, 2000; In Final Form: September 21, 2000

A technique for the manipulation of Langmuir-monolayers at the air/water interface is presented. Optical tweezers are combined with fluorescence and Brewster angle microscopy to produce a system capable of mechanical and thermal handling of monolayers on a micrometer scale. The viscoelastic, electrical, and thermodynamic properties of the monolayer can be determined by analysis of the perturbations of its structure. A method for force and heat calibration of the tweezers is given. Both kinds of micromanipulations are applied to the star shaped condensed domains in liquid expanded surroundings of bis[8-(1,2-dipalmitoyl-sn-glycero-3-phosphoryl)-3,6-dioxaoctyl]disulfide ("thiolipid") monolayers. The stability of the stars and the consequence of their interlocking on the interfacial flow are investigated.

Introduction

Langmuir-monolayers at the air/water interface have been investigated for about 80 years. The first film balance was developed by Langmuir in 1917,[1] and this device remains the central part of any setup used to study monomolecular films at the air/water interface. Various methods have been developed to investigate their electrical,[2] thermodynamic,[3] structural,[4] and viscoelastic[5] properties. For the last 20 years, it has been possible to visualize monolayers either by Brewster angle (BAM)[6,7] or by fluorescence microscopy.[8,9]

Various microstructures can be observed in the phase coexistence regions of the quasi two-dimensional Langmuir monolayers. This is in contrast to 3d-systems, where the coexisting phases are macroscopically separated, to minimize the interfacial energy of the system. This peculiarity of the 2d-system is due to the competition between long-range dipolar interactions of the molecules and the line tension of the phase boundaries. Many of the structures observed on Langmuir-monolayers can be understood using this model.

The flow profile at the interface is determined by the rheological properties of the 2d-monolayer and the 3d-subphase. The ratio of the surface shear viscosity of the monolayer and the viscosity of the subphase defines a characteristic length. Above and below this characteristic length, different flow profiles and relaxation dynamics of nonequilibrated two-dimensional liquid systems are expected. On the larger length scale, the subphase flow dominates, whereas on the smaller length scale, the flow is mainly determined by the rheological properties of the monolayer. Different devices have been developed to investigate the viscosity of Langmuir monolayers. The torsion pendulum knife edge shear rheometer[10] works on a millimeter scale and is sensitive to relatively large surface shear viscosities. Smaller viscosities and structures may be investigated by the shear distortion of liquid condensed (LC) domains in liquid expanded (LE) surroundings using a rotating trough.[11] Heckl, Miller, and Möhwald[12] used an inhomogeneous electrical field around a needle to create electrophoretic motion and distort circular LC-domains. The canal flow experiment[13] allows the observation of the circular, two-dimensional flow profile driven by surface pressure gradients. None of these techniques can be used to manipulate monolayers on the micrometer length scale while leaving the surroundings undisturbed. The device presented in this work, a combination of optical tweezers with fluorescence and Brewster angle microscopy, enables this kind of handling.

In this study, the monolayer is mechanically manipulated using particles with a higher refractive index than their surroundings in a focused laser beam. The forces exerted on these particles are in the range of several pN. In addition, local heating by the focused laser causes temperature gradients that disturb monolayer patterns. The calibration and applications of both techniques are presented.

Experimental Section

A schematic drawing of the combination of tweezers with fluorescence microscopy is shown in Figure 1a. Two simultaneous operations are performed by a 100× water immersion objective, numerical aperture 1.0, built into the bottom of a temperature controlled film balance. First, it projects a fluorescence image of the monolayer onto a SIT camera (Hamamatsu C 3077−01). Fluorescence is excited in the labeled (2% 4-hexadecylamino-7-nitrobenz-2-oxa-1,3-diazole, Molecular Probes) monolayer by a p-polarized argon ion laser (465 nm, 150 mW). The excitation light is blocked by a filter in front of the detector. Second, two IR-laser beams ($\lambda = 1064$ nm, P = 10 mW-2 W), coupled into the optical path using a dichroic mirror (transparent for fluorescence light), are focused by the

* To whom correspondence should be addressed. E-mail: thomas.fischer@mpikg-golm.mpg.de.
[†] Fakultät für Physik, Universität Leipzig.
[‡] Newport GmbH.
[§] CSEM SA.
[||] Laboratoire de Chimie Physique des Polymères et Membranes, Département de Chimie, Ecole Polytechnique Fédérale de Lausanne.
[⊥] Max Planck Institute of Colloids and Interfaces.

10.1021/jp0024266 CCC: $20.00
Published on Web 12/12/2000

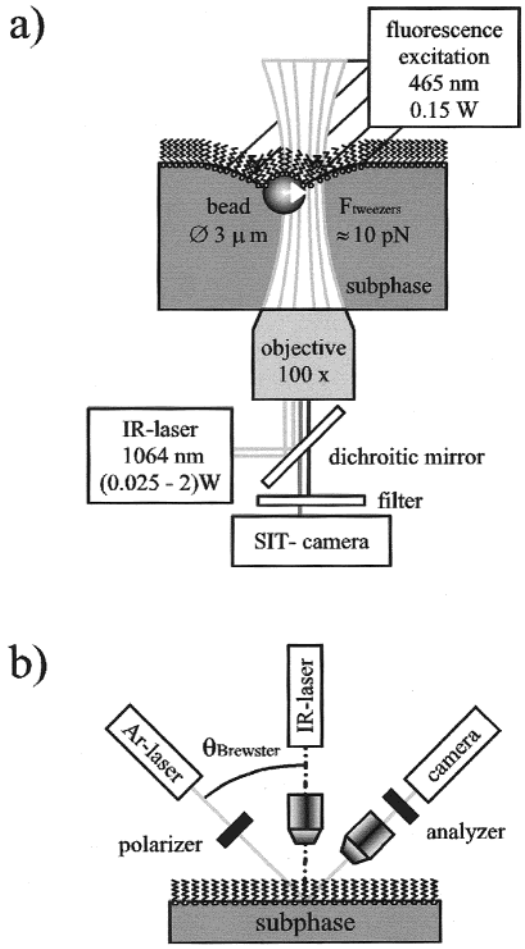

Figure 1. Sketch of (a) fluorescence microscopy combined with optical tweezers (b) Brewster angle microscopy combined with a focused IR-laser.

objective onto the monolayer. The diameter of the beams is fit to the objective entrance in order to maximize the lateral optical forces. Before the beams are reflected at the dichroic mirror, both are focused separately using Galilee optics at the air−water interface, where one of the beams can be moved laterally by two rotating mirrors (not shown in Figure 1).

Only the fixed beam was used for the experiments presented in this paper. The particles spread at the air/water interface were silica beads (chloroform suspension, Polysciences) or PE beads (water/ethanol suspension, Bangs). The silica beads were cleaned by rinsing several times in chloroform.

With Brewster angle microscopy the anisotropy of the monolayer can be visualized without using a fluorescence label. It was used in combination with the IR-laser for local heating experiments (Figure 1b). The IR-laser was focused from above onto the air/water interface using an objective with its optical axis normal to the interface. Because both the BAM-objective and the IR-objective (magnifications: 20×) have to be adjusted onto the same spot and may not touch each other, their numerical aperture is limited to 0.35 and the tweezers' forces are weak. Methyl-octadecanoate (mechanical manipulation) and octadecanol (local heating) purchased from Aldrich were used without further purification.

A. Thermal Manipulation. The high laser power of the tweezers ($P > 200$ mW) causes an observable local heating. This can melt the low-temperature phase of a monolayer to give the high temperature phase in a locally defined region (10 μm $\leq r \leq$ 100 μm). In the beam waist of the laser, a fraction of 10^{-6} of the laser power P is converted into heat. Assuming this heat is dissipated into the subphase by heat conduction only, the rise in temperature within the focus is estimated to be

$$\Delta T = \alpha \frac{3P}{4\pi\kappa_W} \quad (1)$$

Here, $\alpha = 0.1$ cm^{-1} denotes the absorption coefficient of water at $\lambda = 1064$ nm, and $\kappa_W \approx 0.6$ W/m·K, the heat conductivity of water. Equation 1 predicts a rise of $\Delta T = 5$ K at a laser power of $P = 1$ W.

Figure 2 shows two Brewster angle microscope images of the locally heated octadecanol monolayer at surface pressures (a) $\pi_\infty = 13.1$ mN/m and (b) $\pi_\infty = 13.0$ mN/m, respectively, with the surface pressure $\pi_\infty = \pi(T_\infty)$ measured with a Wilhelmy plate placed far from the laser focus [$T_\infty = (20.6 \pm 1)$ °C]. The BAM measurements were performed in the vicinity of the phase transition from the untilted LS(Rot II)-phase (homogeneous gray periphery) to the tilted L_2'-phase (central, inhomogeneous region). The focus of the laser is in the center of the images, where a circular region of radius r_c with a mosaic texture of the tilted L_2'-phase can be seen. After the evolution of this region, the monolayer is in hydrostatic equilibrium and does not flow, i.e., the surface tension of the interface is constant.[14]

$$\sigma[T(r), \Gamma(r)] = \sigma_W[T(r)] - \pi[T(r), \Gamma(r)] \equiv \text{const} \quad (2)$$

where σ denotes the surface tension of the monolayer covered interface, σ_W the surface tension of bare air/water interface, and π the surface pressure. $T(r)$ is the radial temperature profile, and $\Gamma(r)$ the surface concentration of amphiphiles. A first-order expansion of eq 2 yields

$$\left[\frac{d\sigma_W}{dT} - \left(\frac{\partial\pi}{\partial T}\right)_\Gamma\right]\Delta T(r) - \left(\frac{\partial\pi}{\partial\Gamma}\right)_T \Delta\Gamma(r) \equiv 0 \quad (3)$$

where $\Delta T(r) = T(r) - T_\infty$, $\Delta\Gamma(r) = \Gamma(r) - \Gamma_\infty$ and $d\sigma_W/dT = -0.12$ mN/m·K. At the boundary with radius r_c of the region showing the mosaic texture, the surface pressure must be equal to the transition pressure π_c of the L_2'/LS(Rot II)-transition[15,16]

$$\pi_c[T(r_c)] = \pi[T(r_c), \Gamma(r_c)] \quad (4)$$

The L_2'/LS(Rot II) transition pressure $\pi_c(T)$ can be well described by

$$\pi_c(T) = \pi_c(T_\infty) + d\pi_c/dT\cdot(T - T_\infty) \quad (5)$$

with $\pi_c(T_\infty = 20\ °C) = 12.8$ mN/m and $d\pi_c/dT = 0.16$ mN/m·K (cf. ref 16).

Inserting eq 3 and eq 5 into eq 4 one finds

$$\Delta T(r_c) = \frac{\pi_\infty - \pi_c(T_\infty)}{\frac{d\pi_c}{dT} - \frac{d\sigma_W}{dT}} \quad (6)$$

Figure 3 shows the temperature profile normalized with the laser power obtained via eq 6 by varying π_∞. As described by eq 1, the rise in temperature within the focus is about 5 K per 1 W laser power. The temperature profile may be fitted using the stationary solution of the heat conductivity equation $\Delta T \propto 1/r$, if convective transport processes are neglected.

Laser powers on the order of 100 mW were used in experiments, where the monolayer was manipulated with silica beads. The change in temperature did not exceed 0.5 K. Note that the temperature profile was measured at high surface pressures of the monolayer. At these pressures, the monolayer

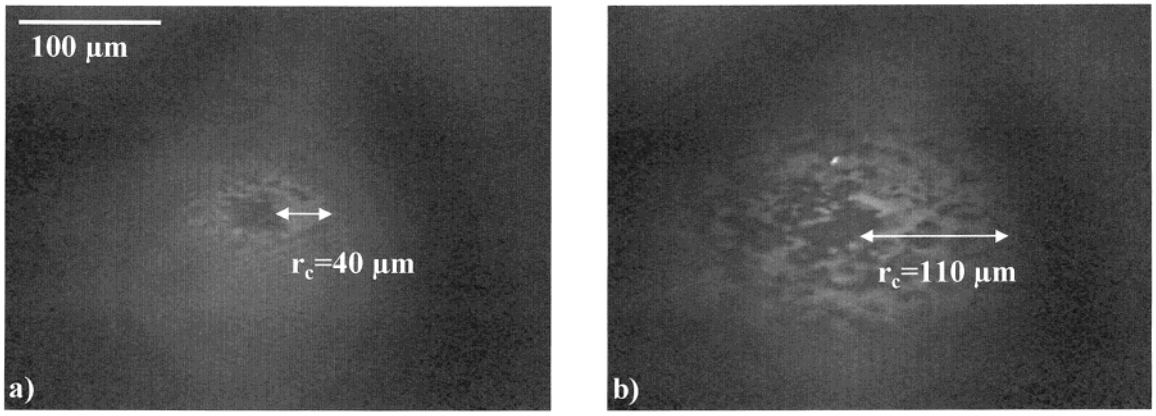

Figure 2. Brewster angle microscope images of an octadecanol monolayer [$T_\infty = (20.6 \pm 1)$°C, (a) $\pi_\infty = (13.1 \pm 0.1)$ mN/m, and (b) $\pi_\infty = (13 \pm 0.1)$ mN/m] locally heated by a focused ($\varnothing \approx 5$ μm) laser beam ($\lambda = 1064$ nm, $P = 700$ mW). A circular region of radius (a) $r_c = (40 \pm 10)$ μm, (b) $r_c = (100 \pm 10)$ μm of the tilted low-pressure L_2'-phase with its typical mosaic texture is observed around the focus. The periphery of this region shows a homogeneous gray value consistent with the untilted high surface pressure LS(Rot II)-phase. The temperatures at r_c calculated with eq 6 are (a) $T = 21.6$ °C and (b) $T = 21.3$ °C.

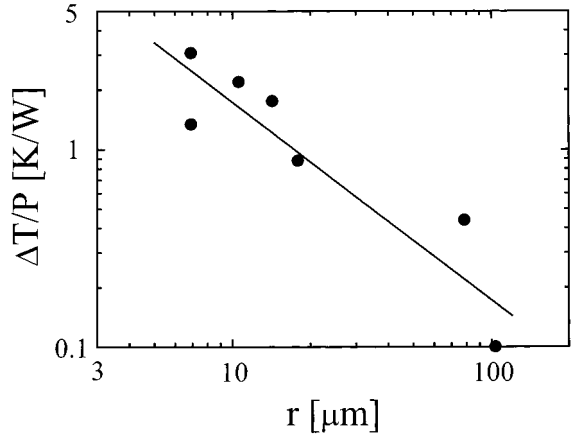

Figure 3. Temperature profile of the monolayer, calculated using eq 6 and normalized to the laser power. The experimental points were obtained by varying the surface pressure π_∞ at a laser power of $P = 800$ mW and measuring the radius r_c of the L_2'-region. The rise in temperature is about 5 K/W within the focus. The temperature profile may be fitted by $\Delta T \propto 1/r$, which applies if heat transport is due to thermal conduction in the absence of convection.

is able to balance surface tension gradients, induced by temperature gradients, with opposite surface pressure gradients, induced by the concentration gradients of the amphiphiles. At lower surface pressures, this compensation is not possible. As a consequence, a Marangoni−Bénard instability[17,18] with a radial velocity pointing from the focus toward the periphery is observed. At the bare air/water interface this convective radial flow can be so strong, that silica beads no longer can be captured with the tweezers.

B. Mechanical Manipulation. The force of the optical tweezers results from the sum of all momentum transfers of the photons passing the water/bead and bead/air interfaces and depends on the position of the bead in the tweezers. For an exact calculation of the force the electromagnetic field in the vicinity of the focus in the presence of the bead must be known. With the addition of the air/water interface near the laser focus, this becomes a difficult problem. The maximum force exerted on such beads in the direction of the beam, in bulk water can be estimated, assuming that approximately 3% of the light pressure actually acts on the bead, one obtains a vertical tweezers force of[19]

$$F_{\text{tweezers}} \approx 0.03(n_W P/c) \qquad (7)$$

where n_w denotes the refractive index of water and c the speed of light. In the case of beads floating at the air/water interface, the lateral optical forces obtained are of the same order of magnitude as those predicted by eq 7. For silica beads as used in our experiments [$\varnothing = (3-10)$ μm], the maximum force exerted by the tweezers is of the order of 0.1 nN at a laser power of 1 W.

The optical force on the beads depends strongly on the location of the air/water interface in the laser focus, so it is important to control the immersion depth of the beads. For beads with radii in the order of micrometers, capillary forces ($F_c \approx 100$ nN) dominate and gravitational forces are negligible; the immersion depth of the bead is controlled by its contact angle with the air/water interface.

Because the tweezers are to be used as an accurate mechanical manipulator, their force must be calibrated. As the contact angle at the particle depends on the system, this has to be performed directly on the monolayer under study. In our experiments, the calibration is performed in the LE/LC phase coexistence region of the monolayer, where the surface pressure (contact angle) is roughly independent of the area per molecule. The silica spheres are adsorbed at the 1d-phase boundaries between coexisting monolayer phases due to dipolar interactions of the beads with the monolayer.[20] With a single silica sphere trapped within the focus of the laser beam, the monolayer phase boundary can be manipulated.[21,22] In Figure 4 , ($t = -0.64$ s) a silica sphere is adsorbed at a methyl-octadecanoate LC-domain ($T = 35$ °C). The tweezers trap the bead with its domain [Figure 4 ($t = -0.36$ s)], while the neighboring domains continue to flow. The force of the tweezers ($P = 150$ mW) may be determined by measuring the velocity of the surrounding LE-phase that is needed to detach the LC-domain with the bead from the tweezers [Figure 4 ($t = 0.08$ s)]. At the detachment velocity ($v = 100 \pm 20$ μm/s, $t = 0$ s) the hydrodynamic drag force equals the force of the tweezers. Given the surface shear viscosity of the LE-phase of methyl-octadecanoate ($\eta_s \ll \eta a$[23,21]), the viscosity of the subphase ($\eta = 0.725$ mPa·s[24]) and the radius [$a = (15 \pm 1)$ μm] of the LC-domain, the hydrodynamic drag force on a solid disk can be calculated[25]

$$\vec{F} = -f\eta a\vec{v} \qquad (8)$$

where

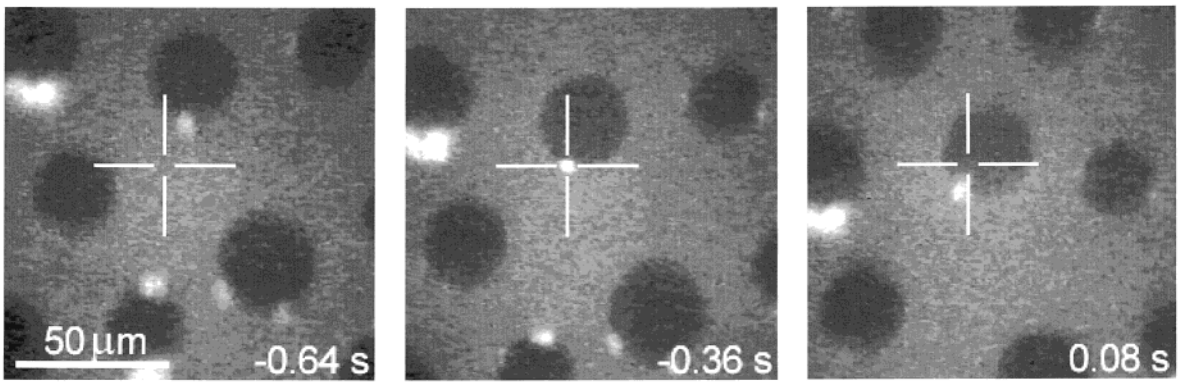

Figure 4. Capture and detachment of a liquid condensed domain of methyl-octadecanoate from the optical tweezers ($P = 150$ mW). (a) The domains are flowing toward the bottom of the image with a velocity of $v = (90 \pm 20)$ μm/s. (b) One domain [$a = (15 \pm 1)$ μm] is trapped within the tweezers. The other domains continue to flow. A slight increase in the velocity [$v_{\text{rupture}} = (100 \pm 20)$ μm/s, $t = 0$ s] detaches the bead with the domain from the tweezers (c). The calculated optical force is $F_{\text{tweezers}} = (9 \pm 2)$ pN.

$$f = \begin{cases} \dfrac{4\pi \mathrm{B}}{\ln(2\mathrm{B}) - 0.577 + \dfrac{4}{\pi \mathrm{B}} - \dfrac{1}{2\mathrm{B}^2}\ln(2\mathrm{B})} & \text{for } \mathrm{B} > 2 \\ 8 & \text{for } \mathrm{B} < 1 \end{cases}$$

The dimensionless friction coefficient, f, depends on the Boussinesq number $B = \eta_s/\eta a$. Here, $B < 7$ and $f = 8$, hence $F_{\text{tweezers}} = (9 \pm 2)$ pN. The calibration procedure described above is valid only for a Newtonian behavior of the surrounding monolayer phase.

C. Examples: Manipulations of Star-Shaped Domains. In Figure 5 the mechanical manipulation of a of bis[8-(1,2-dipalmitoyl-sn-glycero-3-phosphoryl)-3,6-dioxaoctyl]disulfide ("thiolipid") Langmuir-monolayer[26] is shown. In the LC/ LE phase coexistence region, the condensed domains are star shaped (Figure 5a). A captured silica bead hits the edge of one arm of the star and causes it to rotate (Figures 5a-f). In principle, the construction of a two-dimensional gearbox, consisting of 10^9 molecules (1fl), is possible.

In thiolipid films at low densities of LC-domains, direct contact between individual domains rarely occurs. The individual domains are only affected by dipole and hydrodynamic interactions. The flow profile of the domains surroundings around a trapped silica bead is laminar (Figure 6a), as determined by following the trajectories of several domains as they flowed past the trapped bead. A perturbation of the flow of domains is visible in a region reaching approximately 20 μm from the trapped bead.

Compression of the monolayer results in more densely packed LC-stars as shown in Figure 7a. The stars are arranged on a regular hexatic structure. Individual domains still do not touch, but the shear flow around the trapped domain now leads to chains of interlocked stars (Figure 7b; one of the chains is marked in white) in the vicinity of a trapped bead. The original hexatic arrangement is destroyed and the corresponding flow profile is chaotic (Figure 6b). Individual trajectories may cross each other when a pair of stars are meshed and rotate around each other (see the gray trajectory). The meshing leads to long-range steric interactions and a disturbed flow is visible up to 50 μm from the location of the tweezers. The flow is no longer symmetric and changes its direction after passing the tweezers. The critical fraction of the condensed phase at a velocity $v_\infty = (30 \pm 5)$ μm/s, above which the chaotic flow is observable, is $\phi_c(v) = (30 \pm 5)$ %. In 3d, dense colloidal suspensions, shear flow is known to create chaotic trajectories of individual colloidal particles leading to a reduction in density of colloidal particles within the shear zone.[27]

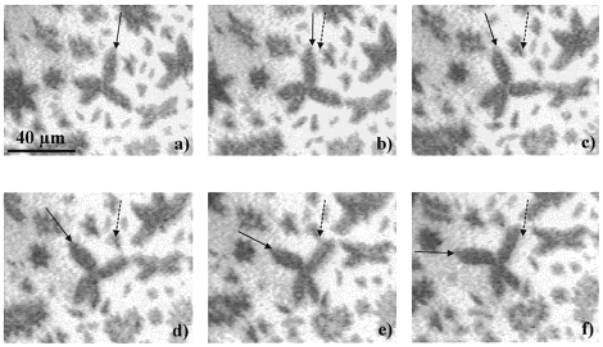

Figure 5. Rotation of a star shaped condensed domain in a thiolipid Langmuir-monolayer using optical tweezers. At this domain density the individual stars do not mesh. The tweezers are located at the black arrow and the dashed arrow indicates the original location.

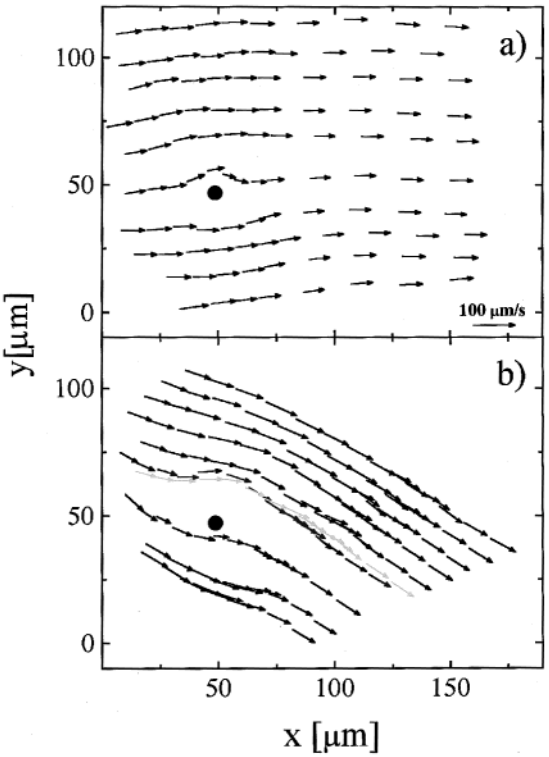

Figure 6. The transition from laminar to a chaotic flow within a thiolipid monolayer: (a) below and (b) above the critical meshing density (the trajectory of one of the two domains that switch positions as they are interlocked is marked by gray arrows to distinguish it from the second crossing trajectory).

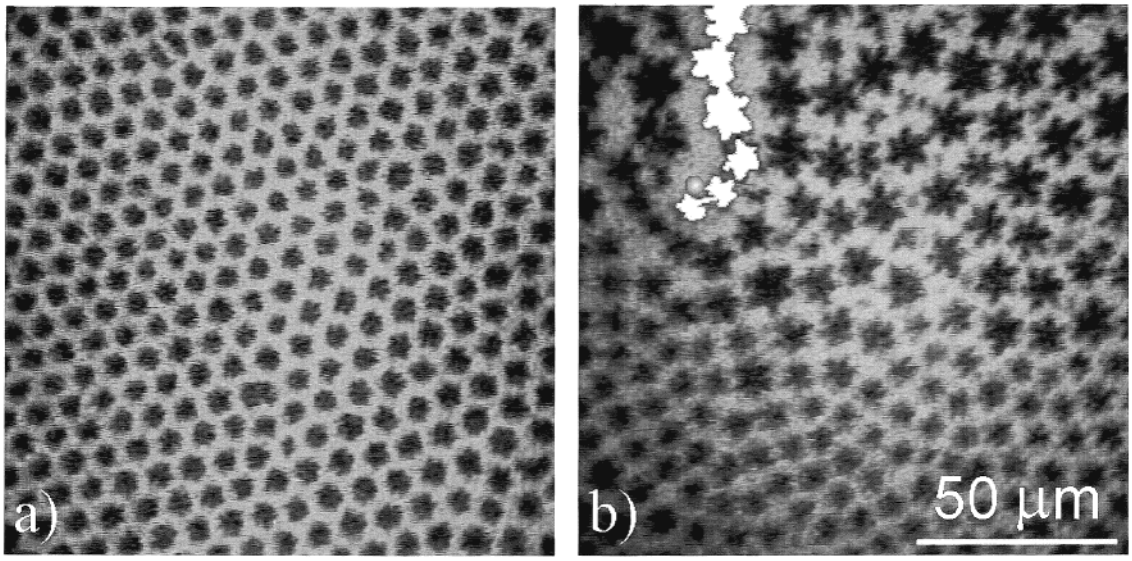

Figure 7. Textures of the LC/LE coexistence region in a thiolipid monolayer: (a) a regular hexatic arrangement of unmeshed domains with the tweezers switched off (b) the formation of interlocked chains (one chain is marked white) as the monolayer flows around the trapped bead.

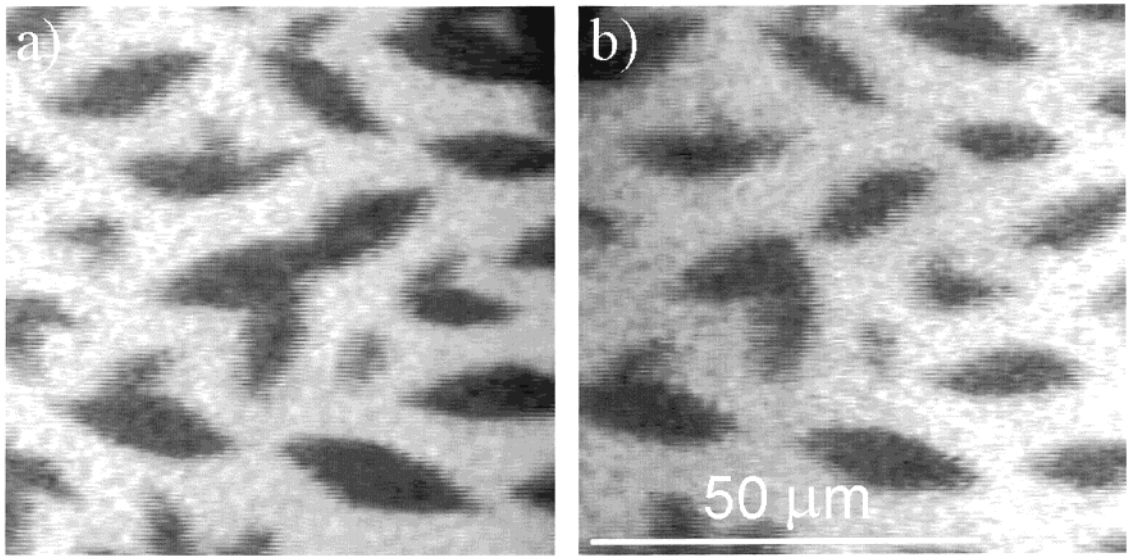

Figure 8. Star of the thiolipid monolayer, close to the instability, (a) before and (b) after passing the local heating. The star in the center has been broken into two parts as the critical strain inside the domain has been reached.

At small domain sizes the star shape is stable. As the size of a domain increases (partly due to surfactant impurities introduced into the monolayer when spreading the beads), a breakup of the star into individual leaf shaped arms is observed. The stability of the star is determined by an interplay of the elastic, dipolar, and line energies. The elastic and dipolar energy parts support the breakup, whereas the line energy stabilizes the star shape. If a critical size of the star is reached, the elastic stress and dipolar forces exceed the line tension and the breakup occurs. In Figure 8a star at the critical size [length of one arm$\approx$-(20 ± 2) μm] is depicted. The small temperature gradient ($\Delta T/\Delta R \approx 10^5$ K/m, $P = 100$ mW) of the local heating increases the elastic strain inside the star and the breakup occurs. The star in the center of Figure 8a, consisting of three arms, is broken into two parts due to the heating (Figure 8b).

Summary

Local thermal and mechanical manipulation techniques capable of deforming coexisting monolayer phases have been presented. These techniques enable the determination of the nature of the interactions between the different phases, the measurement of surface shear viscosities,[23] line tension,[21,22] and dipole density differences.[28] Typical optical forces exerted on trapped particles range from (1−100) pN. In principle the local mechanical manipulation allows the construction of two-dimensional engines consisting of 10^9 molecules (1 fl).

On increasing the domain density within the 2d colloidal systems of bis[8-(1,2-dipalmitoyl-sn-glycero-3-phosphoryl)-3,6-dioxaoctyl]disulfide ("thiolipid"), a transition from laminar to chaotic flow is observed.

Using the focused laser as local heating, defined temperature gradients (up to $\Delta T/\Delta R \approx 10^6$ K/m) can be applied on a local region. This leads to a breakup of the thiolipid domains and can be employed to determine elastic properties of the monolayer phases.

Acknowledgment. We thank Prof. Möhwald for buying both experimental setups from the University of Leipzig. This work

was supported by the German Science foundation within the "Innovationskolleg Phänomene an den Miniaturisierungsgrenzen" and the "priority program wetting and structure formation at interfaces". T.F. thanks the German Science foundation for a Heisenberg fellowship.

References and Notes

(1) Langmuir, I. *J. Am. Chem. Soc.* **1917**, *39*, 1848.
(2) McConnell, H. M. *Annu. Rev. Phys. Chem.* **1991**, *42*, 171.
(3) Albrecht, O. Dissertation, University of Ulm, Ulm, 1979.
(4) Knobler, C. M.; Desai, R. C. *Annu. Rev. Phys. Chem.* **1992**, *43*, 207.
(5) Edwards, D. A.; Brenner, H.; Wasan, D. T. *Interfacial Transport Processes and Rheology*; Butterworth-Heinemann: Boston, 1991.
(6) Hénon, S.; Meunier, J. *Rev. Sci. Instrum.* **1991**, *62*, 936.
(7) Hönig, D.; Möbius, D. *J. Phys. Chem.* **1991**, *95*, 4590.
(8) Lösche, M.; Sackmann, E.; Möhwald, H. *Ber Bunsen-Ges. Phys. Chem.* **1983**, *87*, 848.
(9) McConnell, H. M.; Tann, L. K.; Weiss, R. M. *Proc. Natl. Acad. Sci.* (USA) **1984**, *81*, 3249.
(10) Goodrich, F. C.; Allen, L. H.; Poskanzer, A. *J. Coll. Int. Sci.* **1975**, *52*, 201.
(11) Benvengnu, D. J.; McConnell, H. *J. Phys. Chem.* **1992**, *96*, 6820.
(12) Heckl, W. M.; Miller, A.; Möhwald, H. *Thin Solid Films* **1988**, *159*, 125.
(13) Schwartz, D. K.; Knobler, C. M.; Bruinsma, R. *Phys. Rev. Lett* **1994**, *73*, 2841.
(14) Preliminary experiments seem to indicate that the hexatic liquid condensed phases in octadecanol behave elastic under low shear rates and that it is not always justified to treat the liquid condensed phases as a 2d fluid.
(15) This is strictly valid only if the line tension between the L_2' and LS phase vanishes. It has been shown by Lautz et al. (ref 16) that the transition is of weekly first order. Therefore, the line tension is very low and can be neglected.
(16) Lautz, C.; Fischer, Th. M.; Weygand, M.; Lösche, M.; Kjaer, C.; Howes, P. *J. Chem. Phys.* **1998**, *108*, 4640.
(17) Pearson, J. R. A. *J. Fluid. Mech.* **1958**, *4*, 489.
(18) Scriven, L. E.; Sterling, C. V. *J. Fluid. Mech.* **1964**, *19*, 321.
(19) Block, S. M. Optical Tweezers: A New Tool for Biophysics, in *Noninvasive Techniques in Cell Biology*; Wiley-Liss: New York, 1990; 375−402.
(20) Nassoy, P.; Birch, W. R.; Andelman, D.; Rondelez, F. *Phys. Rev. Lett.* **1996**, *76*, 455.
(21) Wurlitzer, S.; Steffen, P.; Fischer, Th. M. *J. Chem. Phys.* **2000**, *112*, 5915.
(22) Wurlitzer, S.; Steffen, P.; Wurlitzer, M.; Khattari, Z.; Fischer, Th. M. *J. Chem. Phys.* **2000**, *113*, 3822.
(23) Wurlitzer, S.; Fischer, Th. M., in preparation.
(24) *Landolt Börnstein IV/1*, 6th. ed, Springer, Berlin: **1955**, *600*, 613.
(25) Hughes, B. D.; Pailthorpe, B. A.; White, L. R. *J. Fluid Mech.* **1981**, *110*, 349.
(26) Lang, H.; Duschl, C.; Vogel, H. *Langmuir* **1994**, *10*, 197.
(27) Leighton, D.; Acrivos, A. *J. Fluid Mech.* **1987**, *181*, 415.
(28) Heinig, P.; Wurlitzer, S.; Steffen, P.; Kremer, F.; Fischer, Th. M. *Langmuir*, in press.